

Numerical simulation of fracture flow with a mixed-hybrid FEM stochastic discrete fracture network model

Jiří Maryška[†] (jiri.maryska@vslib.cz), Otto Severýn[†]
(otto.severyn@vslib.cz) and Martin Vohralík^{†,‡}
(vohralik@km1.fjfi.cvut.cz)

[†] *Department of Process Modelling, Faculty of Mechatronics and Interdisciplinary Engineering Studies, Technical University of Liberec, Hálkova 6, 461 17 Liberec 1, Czech Republic*

[‡] *Department of Mathematics, Faculty of Nuclear Sciences and Physical Engineering, Czech Technical University in Prague, Trojanova 13, 120 00 Prague 2, Czech Republic*

Abstract.

We introduce a discrete fracture network model of stationary Darcy flow in fractured rocks. We approximate the fractures by a network of planar circle disks, which is generated on the basis of statistical data obtained from field measurements. We then discretize this network into a mesh consisting of triangular elements placed in three-dimensional space. We use geometrical approximations in fracture planes, which allow for a significant simplification of the final triangular meshes. We consider two-dimensional Darcy flow in each fracture. In order to accurately simulate the channeling effect, we assign to each triangle an aperture defining its hydraulic permeability. For the discretization we use the lowest order Raviart–Thomas mixed finite element method. This method gives quite an accurate velocity field, which is computed directly and which satisfies the mass balance on each triangular element. We demonstrate the use of this method on a model problem with a known analytical solution and describe the generation and triangulation of the fracture network and the computation of fracture flow for a particular real situation.

Keywords: fractured medium, Darcy flow, stochastic discrete fracture network model, channeling effect, mixed-hybrid finite element method

1. Introduction

Underground granitoid massifs are proposed as nuclear waste repositories. However, they are always disrupted by a system of geological faults, *fractures*. We study in this paper the percolation of groundwater in such massifs, called *fracture flow*.

According to [4] or [21], there are three main approaches to modeling fracture flow. When only a large-scale model is required and there is no need to know the detailed flow behavior in any site subarea, it is possible to use *equivalent porous medium models*. More complex are *dual porosity models* with two distinct interacting subsystems—



© 2004 Kluwer Academic Publishers. Printed in the Netherlands.

fractures and porous blocks. Finally, we can approximate the original three-dimensional fractures by planar elliptic or polygonal disks whose frequency, size, assigned aperture, and orientation are statistically derived from field measurements and consider two-dimensional Darcy flow in such a network. However, because of the high computer requirements, it is only possible to solve local problems by using *stochastic discrete fracture network models*. We refer to [1] for more details.

In [12, 7, 8] the networks of polygonal disks are replaced by networks of one-dimensional pipes. This allows for fast calculations with large networks, but the precision is compromised. The models proposed in [9, 2, 10, 17, 3] discretize the polygonal networks into triangular or quadrilateral meshes. The numbers of mesh elements are often sizably increased. Finite difference, finite volume, finite element, or boundary element methods are used for the discretization. We refer, for instance, to [5] for a more detailed survey of the stochastic discrete fracture network models proposed in the literature. The intention of this paper is twofold. First, we describe how to construct a very accurate approximation of the fracture network, which has at the same time as few elements as possible. This allows us to represent realistic fractured media while simultaneously decreasing the time of calculations. Second, we propose to use a mixed finite element method for the discretization of the fracture flow problem.

We generate the fracture network on the basis of statistical data obtained from field measurements. We enable the definition of hydraulically important fractures, zones with an increased density of fractures, and the insertion of deterministic fractures. The original three-dimensional fractures are approximated by planar circle disks and each disk is subsequently discretized into a triangular mesh respecting the intersections with its neighbors. In order to simplify the geometrical situation in fracture planes, the computed intersections are slightly moved and stretched. In this way, one obtains a higher-quality mesh; however, the three-dimensional geometrical correspondence vanishes and has to be replaced with an element edges correspondence. Finally, we assign an aperture to each element. Based on this aperture, the hydraulic permeability of the element is set, considering also fracture wall roughness and filling. The classical parallel plate model is thus avoided and the channeling effect is simulated. We can see an example of a simple triangular mesh in Figure 1.

Mixed finite element methods are known to accurately approximate the velocity field and to locally conserve the mass on each element. We have thus decided to use the lowest order Raviart–Thomas mixed finite element method (see [6] or [16]) in order to find an approximate solution of the locally second-order elliptic problem with a discontinuous perme-

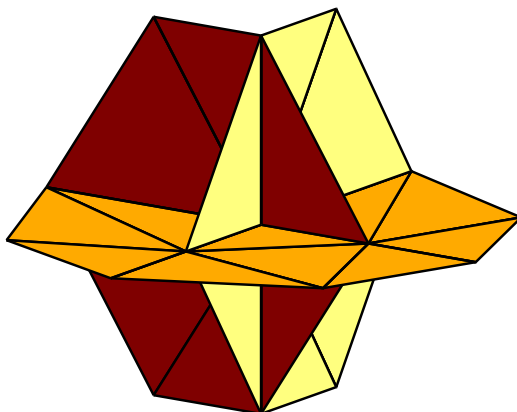


Figure 1. Fracture network made of 3 polygons, discretized into a triangular mesh

ability tensor. We can easily note an essential property of the fracture networks: there exist inter-element edges which belong to three or more triangular elements, see Figure 1. The parallel article [20] (cf. also [19]) is devoted to the problem of the definition of mixed methods for fracture networks. The existence and uniqueness of weak and discrete solutions to our problem, as well as error estimates, follow from this article.

The outline of the paper is as follows. We give the formulation of the problem of stationary Darcy flow in a fracture network in the next section. In Section 3 we define function spaces and the weak and discrete solutions and give error estimates. We sketch the implementation of the lowest order Raviart–Thomas mixed finite element method in the form of the *Fracture Flow Solver* in Section 4. Section 5 is devoted to a numerical experiment with a model problem with a known analytical solution. We describe the generation of fracture networks and their subsequent discretization into triangular meshes by the *Fracture Network Generator* in Sections 6 and 7, respectively. An example of the computation of fracture flow for a real problem is given in Section 8. Finally, in Section 9 we make some concluding remarks.

2. Stationary Darcy flow in a fracture network

We define the *fracture network* \mathcal{S} by

$$\mathcal{S} \equiv \left\{ \bigcup_{\ell \in L} \overline{\alpha_\ell} \setminus \partial \mathcal{S} \right\}, \quad (1)$$

where α_ℓ is an open two-dimensional polygon placed in three-dimensional space. We call $\overline{\alpha_\ell}$, the closure of α_ℓ , a *fracture*. L is the index

set of fractures and $\partial\mathcal{S}$ is the boundary of \mathcal{S} . For the purpose of the mathematical description, we suppose that the fractures are only connected through their boundary edges. We suppose that there is a two-dimensional orthogonal coordinate system given in each fracture. The system \mathcal{S} of the model problem in Figure 2 may serve as an example. In this case \mathcal{S} consists of four fractures α_1 – α_4 and $\partial\mathcal{S}$ consists of twelve edges Λ_1 – Λ_{12} .

We seek the fracture flow velocity \mathbf{u} (a two-dimensional vector in each α_ℓ), which is the solution of the problem

$$\mathbf{u} = -\mathbf{K}(\nabla p + \nabla z) \quad \text{in } \mathcal{S}, \quad (2a)$$

$$\nabla \cdot \mathbf{u} = q \quad \text{in } \mathcal{S}, \quad (2b)$$

$$p = p_D \quad \text{on } \Lambda_D, \quad \mathbf{u} \cdot \mathbf{n} = u_N \quad \text{on } \Lambda_N, \quad (2c)$$

where all the variables are expressed in the local coordinates of appropriate α_ℓ and also the differentiation is always done with respect to these local coordinates. The equation (2a) is Darcy's law, (2b) is the mass balance equation, and (2c) prescribes Dirichlet and Neumann boundary conditions. The variable p denotes the piezometric head, $p = \frac{\tilde{p}}{\rho g}$, where \tilde{p} is the fluid pressure, g is the gravitational acceleration constant, and ρ is the fluid density, q represents stationary sources or sinks density, and z is the elevation, i.e. the upward vertical three-dimensional coordinate. The second-rank tensor \mathbf{K} of hydraulic conductivity is a function of the original three-dimensional fracture aperture, wall roughness, and filling. We suppose that \mathbf{K} is symmetric and uniformly positive definite on each α_ℓ . We finally require that $\Lambda_D \cap \Lambda_N = \emptyset$, $\overline{\Lambda_D} \cup \overline{\Lambda_N} = \partial\mathcal{S}$, and $\Lambda_D \neq \emptyset$.

3. Mixed-hybrid finite element method

We give in this section the definitions of continuous and discrete function spaces on the system of fractures \mathcal{S} . We then state the weak mixed solution, mixed-hybrid approximation, and give error estimates.

3.1. FUNCTION SPACES

We use the product of L^2 spaces on individual fractures in order to define the $L^2(\mathcal{S})$ and $\mathbf{L}^2(\mathcal{S})$ spaces on the system \mathcal{S} ,

$$L^2(\mathcal{S}) \equiv \prod_{\ell \in L} L^2(\alpha_\ell) \quad , \quad \mathbf{L}^2(\mathcal{S}) \equiv L^2(\mathcal{S}) \times L^2(\mathcal{S}). \quad (3)$$

For each fracture $\overline{\alpha_\ell}$, we denote by $H^1(\alpha_\ell)$ the Sobolev space of scalar functions with square-integrable weak derivatives, $H^1(\alpha_\ell) = \{\varphi \in L^2(\alpha_\ell); \nabla\varphi \in \mathbf{L}^2(\alpha_\ell)\}$. We define $H^1(\mathcal{S})$ as the space of functions whose restrictions on each α_ℓ are from $H^1(\alpha_\ell)$ and which coincide on inter-fracture boundaries in the sense of traces,

$$\begin{aligned} H^1(\mathcal{S}) \equiv & \left\{ v \in L^2(\mathcal{S}); v|_{\alpha_\ell} \in H^1(\alpha_\ell) \quad \forall \ell \in L, \right. \\ & \left. (v|_{\alpha_i})|_f = (v|_{\alpha_j})|_f \quad \forall f = \overline{\alpha_i} \cap \overline{\alpha_j}, i, j \in L \right\}. \end{aligned} \quad (4)$$

We then have the spaces $H^{\frac{1}{2}}(\partial\mathcal{S})$, $H^{-\frac{1}{2}}(\partial\mathcal{S})$, and the space $H_D^1(\mathcal{S})$ of the functions from $H^1(\mathcal{S})$ vanishing on Λ_D as in the standard planar case.

For each fracture $\overline{\alpha_\ell}$, we denote by $\mathbf{H}(\text{div}, \alpha_\ell)$ the space of vector functions with square-integrable weak divergences, $\mathbf{H}(\text{div}, \alpha_\ell) = \{\mathbf{v} \in \mathbf{L}^2(\alpha_\ell); \nabla \cdot \mathbf{v} \in L^2(\alpha_\ell)\}$. We define $\mathbf{H}(\text{div}, \mathcal{S})$ as the space of functions whose restrictions on each α_ℓ are from $\mathbf{H}(\text{div}, \alpha_\ell)$ and whose sum of normal traces over all fractures sharing the given interior edge f is zero in the appropriate sense,

$$\begin{aligned} \mathbf{H}(\text{div}, \mathcal{S}) \equiv & \left\{ \mathbf{v} \in \mathbf{L}^2(\mathcal{S}); \mathbf{v}|_{\alpha_\ell} \in \mathbf{H}(\text{div}, \alpha_\ell) \quad \forall \ell \in L, \right. \\ & \left. \sum_{i \in I_f} \langle \mathbf{v}|_{\alpha_i} \cdot \mathbf{n}_{\partial\alpha_i}, \varphi_i \rangle_{\partial\alpha_i} = 0, \forall f \text{ such that } |I_f| \geq 2, \right. \\ & \left. \forall \varphi_i \in H_{\partial\alpha_i \setminus f}^1(\alpha_i), I_f = \{i \in L; f \subset \partial\alpha_i\} \right\}. \end{aligned} \quad (5)$$

Finally, we denote

$$\mathbf{H}_{0,N}(\text{div}, \mathcal{S}) \equiv \left\{ \mathbf{v} \in \mathbf{H}(\text{div}, \mathcal{S}); \langle \mathbf{v} \cdot \mathbf{n}, \varphi \rangle_{\partial\mathcal{S}} = 0 \quad \forall \varphi \in H_D^1(\mathcal{S}) \right\}$$

as the space of functions from $\mathbf{H}(\text{div}, \mathcal{S})$ such that their normal trace on Λ_N is equal to zero in the appropriate sense.

We use $(\cdot, \cdot)_{0, \alpha_\ell}$ to denote the L^2 scalar product, $\|\cdot\|_{0, \alpha_\ell}$ to denote the associated L^2 norm, $\|\cdot\|_{1, \alpha_\ell}$ to denote the $H^1(\alpha_\ell)$ norm, and $\|\cdot\|_{\mathbf{H}(\text{div}, \alpha_\ell)}$ to denote the $\mathbf{H}(\text{div}, \alpha_\ell)$ norm given by $\|\mathbf{v}\|_{\mathbf{H}(\text{div}, \alpha_\ell)}^2 = \|\mathbf{v}\|_{0, \alpha_\ell}^2 + \|\nabla \cdot \mathbf{v}\|_{0, \alpha_\ell}^2$. The bracket $\langle \mathbf{v} \cdot \mathbf{n}, \varphi \rangle_{\partial\mathcal{S}}$ denotes the duality pairing between $H^{-\frac{1}{2}}(\partial\mathcal{S})$ and $H^{\frac{1}{2}}(\partial\mathcal{S})$ and may be written formally as $\int_{\partial\mathcal{S}} \mathbf{v} \cdot \mathbf{n} \varphi \, ds$. The norms on the spaces defined by (3), (4), (5) are given by

$$\|\cdot\|_{\cdot, \mathcal{S}}^2 = \sum_{\ell \in L} \|\cdot\|_{\cdot, \alpha_\ell}^2.$$

Remark. The definitions (4) and (5) coincide with the characterizations of the spaces $H^1(\mathcal{S})$ and $\mathbf{H}(\text{div}, \mathcal{S})$ for the standard planar case,

see [16, Theorem 1.3]. Note that (4) ensures the appropriate continuity of a scalar function also for fracture networks. Similarly, (5) ensures the continuity of the normal trace of a vector function, i.e. the mass balance condition, even if the interior edge is shared by three or more fractures. Simply, what is the outflow from one fracture has to be the inflow into the neighboring ones.

We now introduce the discrete spaces. Let us suppose a triangulation \mathcal{T}_h of the system \mathcal{S} . For a given triangular element e , we define $\mathbf{RT}^0(e)$ as the space of linear vector functions with the basis \mathbf{v}_i^e , $i \in \{1, 2, 3\}$,

$$\mathbf{v}_i^e = \frac{1}{2|e|} \begin{pmatrix} x - x_i \\ y - y_i \end{pmatrix},$$

where $|e|$ is the area of the element e and $[x_i, y_i]$ are the coordinates of its i -th vertex. The Raviart–Thomas space $\mathbf{RT}_{-1}^0(\mathcal{T}_h)$ of elementwise linear vector functions without any continuity requirement is defined by

$$\mathbf{RT}_{-1}^0(\mathcal{T}_h) \equiv \{ \mathbf{v} \in \mathbf{L}^2(\mathcal{S}); \mathbf{v}|_e \in \mathbf{RT}^0(e) \quad \forall e \in \mathcal{T}_h \}. \quad (6)$$

The space $M_{-1}^0(\mathcal{T}_h)$ of elementwise constant scalar functions is defined by

$$M_{-1}^0(\mathcal{T}_h) \equiv \{ \phi \in L^2(\mathcal{S}); \phi|_e \text{ is constant } \forall e \in \mathcal{T}_h \}. \quad (7)$$

We denote the set of all edges by Λ_h and the set of all edges except those from Λ_D by $\Lambda_{h,D}$, $\Lambda_{h,D} = \Lambda_h \setminus \Lambda_D$. On $\Lambda_{h,D}$ we set

$$M_{-1}^0(\Lambda_{h,D}) \equiv \{ \mu : \Lambda_h \rightarrow \mathbb{R}; \mu|_f \text{ is constant } \forall f \in \Lambda_h, \\ \mu|_f = 0 \quad \forall f \in \Lambda_D \}. \quad (8)$$

3.2. WEAK MIXED SOLUTION

We now define the weak mixed solution of the problem (2a)–(2c). We denote $\mathbf{A} = \mathbf{K}^{-1}$ on each α_ℓ , characterizing the medium resistance. Let us consider $\tilde{\mathbf{u}} \in \mathbf{H}(\text{div}, \mathcal{S})$ such that $\tilde{\mathbf{u}} \cdot \mathbf{n} = u_N$ on Λ_N in the appropriate sense.

DEFINITION 1. *As the weak mixed solution of the steady saturated fracture flow problem (2a)–(2c), we understand functions $\mathbf{u} = \mathbf{u}_0 + \tilde{\mathbf{u}}$, $\mathbf{u}_0 \in \mathbf{H}_{0,N}(\text{div}, \mathcal{S})$, and $p \in L^2(\mathcal{S})$ satisfying*

$$(\mathbf{A}\mathbf{u}_0, \mathbf{v})_{0,\mathcal{S}} - (\nabla \cdot \mathbf{v}, p)_{0,\mathcal{S}} = -\langle \mathbf{v} \cdot \mathbf{n}, p_D \rangle_{\partial\mathcal{S}} + (\nabla \cdot \mathbf{v}, z)_{0,\mathcal{S}} \quad (9a) \\ -\langle \mathbf{v} \cdot \mathbf{n}, z \rangle_{\partial\mathcal{S}} - (\mathbf{A}\tilde{\mathbf{u}}, \mathbf{v})_{0,\mathcal{S}} \quad \forall \mathbf{v} \in \mathbf{H}_{0,N}(\text{div}, \mathcal{S}),$$

$$-(\nabla \cdot \mathbf{u}_0, \phi)_{0,\mathcal{S}} = -(q, \phi)_{0,\mathcal{S}} + (\nabla \cdot \tilde{\mathbf{u}}, \phi)_{0,\mathcal{S}} \quad \forall \phi \in L^2(\mathcal{S}). \quad (9b)$$

We require $\mathbf{A}_{ij} \in L^\infty(\mathcal{S})$, $q \in L^2(\mathcal{S})$, $p_D \in H^{\frac{1}{2}}(\Lambda_D)$, and $u_N \in H^{-\frac{1}{2}}(\Lambda_N)$.

The existence and uniqueness of the solution of (9a)–(9b) is shown in [20].

3.3. MIXED-HYBRID APPROXIMATION

We now introduce the mixed-hybrid finite element approximation of (9a)–(9b).

DEFINITION 2. *As the hybridization of the lowest order Raviart–Thomas mixed finite element approximation of the problem (9a)–(9b), we understand functions $\mathbf{u}_h = \mathbf{u}_{0,h} + \tilde{\mathbf{u}}$, $\mathbf{u}_{0,h} \in \mathbf{RT}_{-1}^0(\mathcal{T}_h)$, $p_h \in M_{-1}^0(\mathcal{T}_h)$, and $\lambda_h \in M_{-1}^0(\Lambda_{h,D})$ satisfying*

$$\begin{aligned} & \sum_{e \in \mathcal{T}_h} \left\{ (\mathbf{A}\mathbf{u}_{0,h}, \mathbf{v}_h)_{0,e} - (\nabla \cdot \mathbf{v}_h, p_h)_{0,e} + \langle \mathbf{v}_h \cdot \mathbf{n}, \lambda_h \rangle_{\partial e \cap \Lambda_{h,D}} \right\} \\ = & \sum_{e \in \mathcal{T}_h} \left\{ -\langle \mathbf{v}_h \cdot \mathbf{n}, p_D \rangle_{\partial e \cap \Lambda_D} + (\nabla \cdot \mathbf{v}_h, z)_{0,e} - \langle \mathbf{v}_h \cdot \mathbf{n}, z \rangle_{\partial e \cap \partial \mathcal{S}} \right. \\ & \left. - (\mathbf{A}\tilde{\mathbf{u}}, \mathbf{v}_h)_{0,e} \right\} \quad \forall \mathbf{v}_h \in \mathbf{RT}_{-1}^0(\mathcal{T}_h), \end{aligned} \quad (10a)$$

$$\begin{aligned} - \sum_{e \in \mathcal{T}_h} (\nabla \cdot \mathbf{u}_{0,h}, \phi_h)_{0,e} = & - \sum_{e \in \mathcal{T}_h} \left\{ (q, \phi_h)_{0,e} - (\nabla \cdot \tilde{\mathbf{u}}, \phi_h)_{0,e} \right\} \\ & \forall \phi_h \in M_{-1}^0(\mathcal{T}_h), \end{aligned} \quad (10b)$$

$$\sum_{e \in \mathcal{T}_h} \langle \mathbf{u}_{0,h} \cdot \mathbf{n}, \mu_h \rangle_{\partial e \cap \Lambda_{h,D}} = 0 \quad \forall \mu_h \in M_{-1}^0(\Lambda_{h,D}). \quad (10c)$$

It is immediate that if $\mathbf{v}_h \in \mathbf{RT}_{-1}^0(\mathcal{T}_h)$, then $\mathbf{v}_h \in \mathbf{H}_{0,N}(\text{div}, \mathcal{S})$ if and only if

$$\sum_{e \in \mathcal{T}_h} \langle \mathbf{v}_h \cdot \mathbf{n}, \lambda_h \rangle_{\partial e \cap \Lambda_{h,D}} = 0 \quad \forall \lambda_h \in M_{-1}^0(\Lambda_{h,D}).$$

Equation (10c) thus ensures the continuity of the normal trace of the velocity field (mass balance condition) even for fracture networks. The demonstration of the existence and uniqueness of the solution of the problem (10a)–(10c) is given in [20].

3.4. ERROR ESTIMATES

We now give two error estimates. If the solution (\mathbf{u}, p) of (9a)–(9b) is smooth enough and if $(\mathbf{u}_h, p_h, \lambda_h)$ is the solution of (10a)–(10c), we have

$$\|\mathbf{u} - \mathbf{u}_h\|_{\mathbf{H}(\text{div}, \mathcal{S})} + \|p - p_h\|_{0, \mathcal{S}} \leq Ch(\|p\|_{1, \mathcal{S}} + \|\mathbf{u}\|_{1, \mathcal{S}} + \|q\|_{1, \mathcal{S}}),$$

where the constant C does not depend on h (see [6, Proposition IV.1.2]).

Using the piecewise linear but nonconforming approximation p_h^* given by the values of the Lagrange multiplier λ_h in the midpoints of the edges, we have (see [6, Theorem V.3.1])

$$\|p - p_h^*\|_{0, \mathcal{S}} \leq Ch^2(\|p\|_{1, \mathcal{S}} + \|\mathbf{u}\|_{1, \mathcal{S}} + \|q\|_{1, \mathcal{S}}).$$

4. Implementation

Original software called *Fracture Flow Solver* was developed as the implementation of the introduced mixed-hybrid model. It works with fracture networks discretized into triangular meshes, where the inter-element edges are possibly shared by more than two elements. It also works with meshes with no real geometrical correspondence, i.e. when the triangulations of two intersecting fractures do not match along the intersection line. This is necessary for the use of geometrical simplifications in fracture planes, see Figures 4 and 5 and the description in Section 7.

The resulting matrix problem has the form

$$\begin{array}{rcl} \mathbb{A}U + \mathbb{B}P + \mathbb{C}\Lambda & = & \mathbf{q}_1 \\ \mathbb{B}^T U & = & \mathbf{q}_2 \\ \mathbb{C}^T U & = & \mathbf{q}_3 \end{array} .$$

There can be more than two 1's in one column of the submatrix \mathbb{C} , unlike in the classical planar case. This represents an interior edge shared by more than two elements. We have used the solver GI8 of the Institute of Computer Science, Academy of Sciences of the Czech Republic, see [14] or [15] for its description. This solver is based on the sequential elimination onto a system with Schur's complement and subsequent solution of this system by a preconditioned conjugate gradients method.

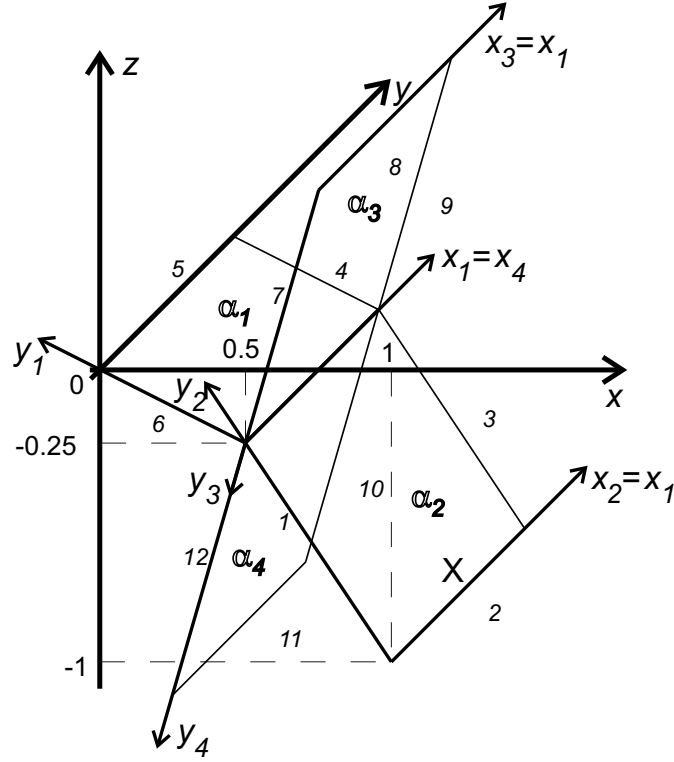


Figure 2. Fracture network of the model problem

5. Model problem

In this section we consider a simple model problem of the form

$$\mathcal{S} = \overline{\alpha_1} \cup \overline{\alpha_2} \cup \overline{\alpha_3} \cup \overline{\alpha_4} \setminus \partial \mathcal{S},$$

$$\begin{aligned} \mathbf{u} &= -(\nabla p + \nabla z) \quad \text{in } \mathcal{S}, \\ \nabla \cdot \mathbf{u} &= 0 \quad \text{in } \mathcal{S}, \end{aligned}$$

$$\begin{aligned} p &= 0 \quad \text{on } \Lambda_1, \quad p = 0 \quad \text{on } \Lambda_2, \\ \mathbf{u} \cdot \mathbf{n} &= 0 \quad \text{on } \Lambda_3, \quad \mathbf{u} \cdot \mathbf{n} = 0 \quad \text{on } \Lambda_4, \\ p &= \sin\left(\frac{\pi x_1}{2X}\right) \sinh\left(\frac{\pi(A+B)}{2X}\right) + SA \quad \text{on } \Lambda_5, \quad p = Sy_1 \quad \text{on } \Lambda_6, \\ p &= 0 \quad \text{on } \Lambda_7, \quad p = 0 \quad \text{on } \Lambda_8, \\ \mathbf{u} \cdot \mathbf{n} &= 0 \quad \text{on } \Lambda_9, \quad \mathbf{u} \cdot \mathbf{n} = 0 \quad \text{on } \Lambda_{10}, \\ p &= \sin\left(\frac{\pi x_4}{2X}\right) \sinh\left(\frac{\pi(B+B)}{2X}\right) \quad \text{on } \Lambda_{11}, \quad p = 0 \quad \text{on } \Lambda_{12}, \end{aligned}$$

where $A = |\Lambda_4| = \frac{\sqrt{5}}{4}$, $X = |\Lambda_2| = 1$, $B = |\Lambda_3| = |\Lambda_9| = |\Lambda_{10}| = \frac{\sqrt{13}}{4}$, and $S = \frac{\partial z}{\partial y_2} - \frac{\partial z}{\partial y_1}$. The fracture network is viewed in Figure 2. The exact solution can be found as

$$\begin{aligned}
p|_{\alpha_1} &= \sin\left(\frac{\pi x_1}{2X}\right) \sinh\left(\frac{\pi(y_1 + B)}{2X}\right) + S y_1, \\
\mathbf{u}|_{\alpha_1} &= \left(-\frac{\pi}{2X} \cos\left(\frac{\pi x_1}{2X}\right) \sinh\left(\frac{\pi(y_1 + B)}{2X}\right), \right. \\
&\quad \left. -\frac{\pi}{2X} \sin\left(\frac{\pi x_1}{2X}\right) \cosh\left(\frac{\pi(y_1 + B)}{2X}\right) - S - \frac{\partial z}{\partial y_1}\right), \\
p|_{\alpha_2} &= \sin\left(\frac{\pi x_2}{2X}\right) \sinh\left(\frac{\pi y_2}{2X}\right), \\
\mathbf{u}|_{\alpha_2} &= \left(-\frac{\pi}{2X} \cos\left(\frac{\pi x_2}{2X}\right) \sinh\left(\frac{\pi y_2}{2X}\right), \right. \\
&\quad \left. -\frac{\pi}{2X} \sin\left(\frac{\pi x_2}{2X}\right) \cosh\left(\frac{\pi y_2}{2X}\right) - \frac{\partial z}{\partial y_2}\right), \\
p|_{\alpha_3} &= \sin\left(\frac{\pi x_3}{2X}\right) \sinh\left(\frac{\pi y_3}{2X}\right), \\
\mathbf{u}|_{\alpha_3} &= \left(-\frac{\pi}{2X} \cos\left(\frac{\pi x_3}{2X}\right) \sinh\left(\frac{\pi y_3}{2X}\right), \right. \\
&\quad \left. -\frac{\pi}{2X} \sin\left(\frac{\pi x_3}{2X}\right) \cosh\left(\frac{\pi y_3}{2X}\right) - \frac{\partial z}{\partial y_3}\right), \\
p|_{\alpha_4} &= \sin\left(\frac{\pi x_4}{2X}\right) \sinh\left(\frac{\pi(y_4 + B)}{2X}\right), \\
\mathbf{u}|_{\alpha_4} &= \left(-\frac{\pi}{2X} \cos\left(\frac{\pi x_4}{2X}\right) \sinh\left(\frac{\pi(y_4 + B)}{2X}\right), \right. \\
&\quad \left. -\frac{\pi}{2X} \sin\left(\frac{\pi x_4}{2X}\right) \cosh\left(\frac{\pi(y_4 + B)}{2X}\right) - \frac{\partial z}{\partial y_4}\right).
\end{aligned}$$

Note the occurrence of the term S ensuring the continuity of the normal trace of the velocity field; the gradients of z in α_1 and α_2 are different.

The following table gives approximation errors in the first fracture α_1 . The fracture network is discretized into $4 \times 2N^2$ regular triangular elements, $h \approx \frac{1}{N}$. There is the expected $O(h)$ convergence of the velocity, $O(h)$ convergence of the original elementwise constant piezometric head, and $O(h^2)$ convergence of the elementwise linear but discontinuous piezometric head. We refer to [20] for a comparison of the mixed-hybrid finite element method on standard two-dimensional domains and on fracture networks with multiply shared inter-element edges.

Table I. Piezometric head and velocity errors in α_1

N	# triangles	$\ p - p_h\ _{0,S}$	$\ p - p_h^*\ _{0,S}$	$\ \mathbf{u} - \mathbf{u}_h\ _{\mathbf{H}(\text{div}, \mathcal{T}_h)}$
2	8×4	0.4445	0.1481	1.2247
4	32×4	0.2212	0.0389	0.6263
8	128×4	0.1102	0.0098	0.3150
16	512×4	0.0550	0.0025	0.1577
32	2048×4	0.0275	6.18·10 ⁻⁴	0.0789
64	8192×4	0.0138	1.54·10 ⁻⁴	0.0394
128	32768×4	0.0069	3.87·10 ⁻⁵	0.0197
256	131072×4	0.0034	9.73·10 ⁻⁶	0.0099

6. Fracture networks generation

In order to generate fracture networks, original software called *Fracture Network Generator* was developed. Each fracture (originally a three-dimensional object) is approximated by a flat circle disk characterized by its *middle coordinates, radius, orientation, hydraulic permeability or aperture distribution, and wall roughness*. Fractures are divided into four *sets*: *fractures in fracture zones, deterministically measured single fractures, hydraulically important fractures, and common fractures*. Fractures are further supposed to be divided into three *types* according to their mean orientation in the three-dimensional cartesian coordinates: $[0,0,1]$, $[0,1,0]$, or $[1,0,0]$. Each combination of set and type, except for deterministically measured single fractures, is treated as an independent statistical population. The *fracture frequency* is defined as the number of fractures per one depth unit in each part of the simulated domain. *Fracture lengths* are supposed to be lognormally distributed (cf. [7]), i.e. with the probability density function

$$f(x) = \frac{1}{\sigma\sqrt{2\pi}x} \exp\left(-\frac{1}{2}\left(\frac{\ln x - \mu}{\sigma}\right)^2\right).$$

Here, μ is the mean of the logarithm and σ is the standard deviation of the logarithm of fracture lengths. Fractures are supposed to have the Fisher-von-Mises distribution of *orientations* around the mean orientations. The probability density function is given by

$$f(\alpha) = \frac{k}{\exp(k)} \exp(k \cos \alpha) \sin \alpha,$$

where α is the angle between the fracture normal vector and the vector of its mean orientation and k is a parameter.

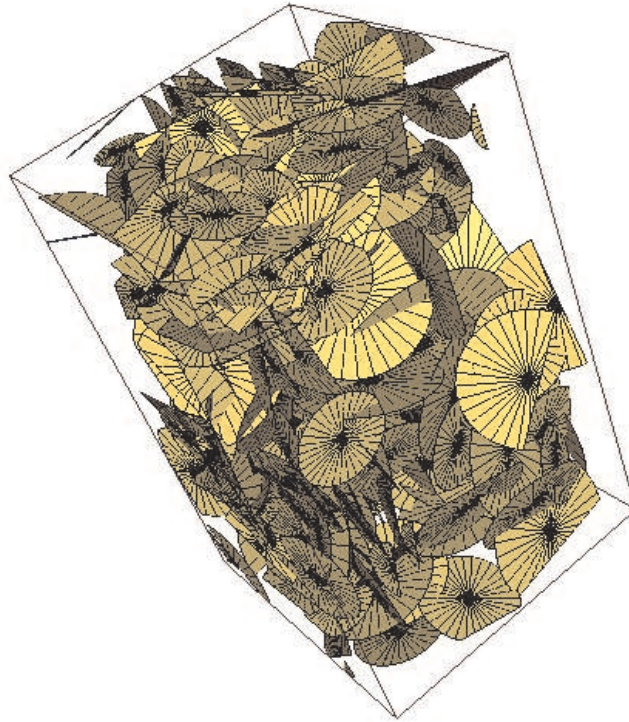


Figure 3. Generated fracture network in a $5 \times 5 \times 8$ m domain

The user has to specify the domain, deterministic single fractures, position of fracture zones, and all statistical parameters. The generator first generates fractures into the fracture zones and then common fractures into the remaining part of the domain. Finally, a network of hydraulically important fractures is generated into the whole domain. One can later add fractures or change the parameters of already generated fractures. For an example of a generated network see Figure 3.

In order to validate the methods used for the statistical description and generation algorithms, χ^2 tests were carried out. One has to strictly distinguish between the statistical distributions and in 'exploration boreholes' measured distributions. The latter are affected by a selective effect. Indeed, while 'drilling a borehole', the probability of intersecting a larger fracture is higher than that of intersecting a smaller one.

7. Final triangular meshes construction

The discretization of fracture networks into triangular meshes has presented a crucial problem. First, each fracture has to be discretized into a triangular mesh respecting the intersections with other fractures. In order to decrease the number of elements and to avoid ill-conditioned matrices resulting from the cases where there exist elements with very small angles, the algorithm should in addition simplify the geometrical situation. In the *Fracture Network Generator*, originally developed discretization algorithm is implemented. It consists of a *preliminary phase* and of an Algorithm for Triangulation of a Polygonal Domain with Pre-defined Interface Lines (*triangulation algorithm*).

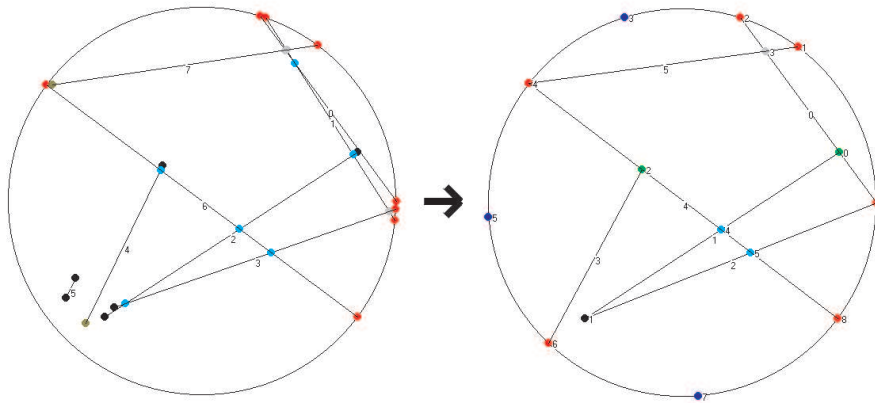


Figure 4. Geometrical simplifications—moving and stretching intersections in the fracture planes

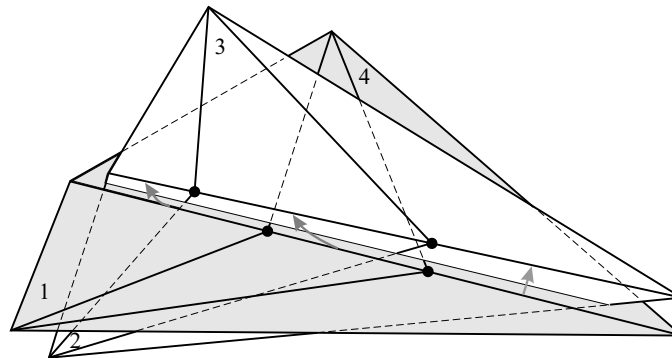


Figure 5. Three-dimensional consequences of geometrical simplifications in the fracture planes

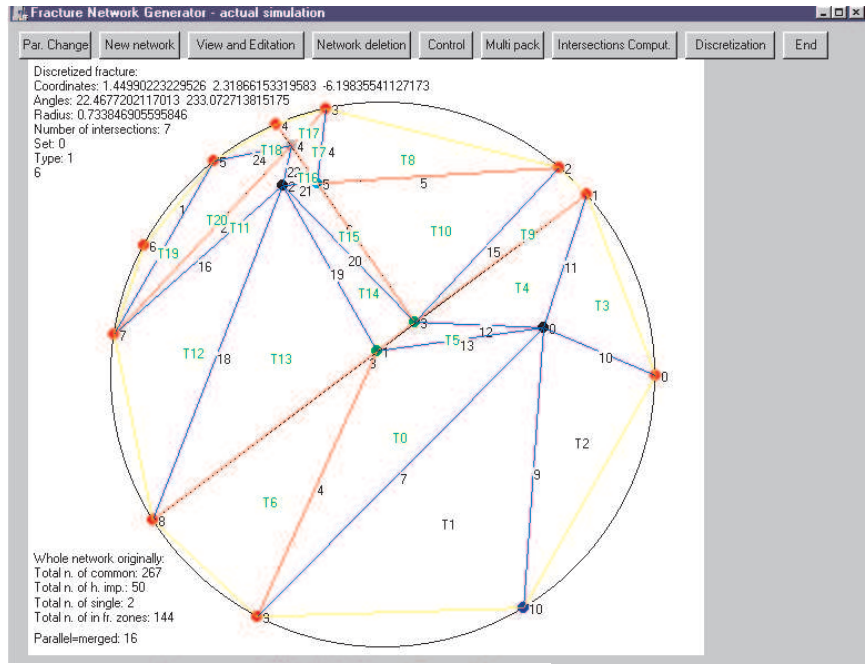


Figure 6. Final discretization of a random fracture

In the preliminary phase identification, intersections computation, and various geometrical simplifications are made. Close, almost parallel fractures are removed or equivalently replaced. In each fracture the computed intersections are moved and stretched in order to simplify the two-dimensional geometrical situation. We can see an example of these simplifications in Figure 4. If the simplifications are used, then the three-dimensional geometrical correspondence vanishes, see Figure 5. It is then replaced with an element edges correspondence stating which triangular element through which edge ensures the communication of its fracture with another fracture, more specifically with which element of this fracture and through which edge. The edges of neighboring elements are then not geometrically identical; the only condition is that the outflow from one triangle has to be the inflow into the connected ones.

The triangulation algorithm is based on combining the *Domain Decomposition Conception* expressing that the domain is split into two parts along an intersection whenever possible and the *Advancing Front Method*. Many user settings influencing the ratio between the precision and the complexity of final triangulations are possible. For an example of the final triangulation of a random circle disk see Figure 6.

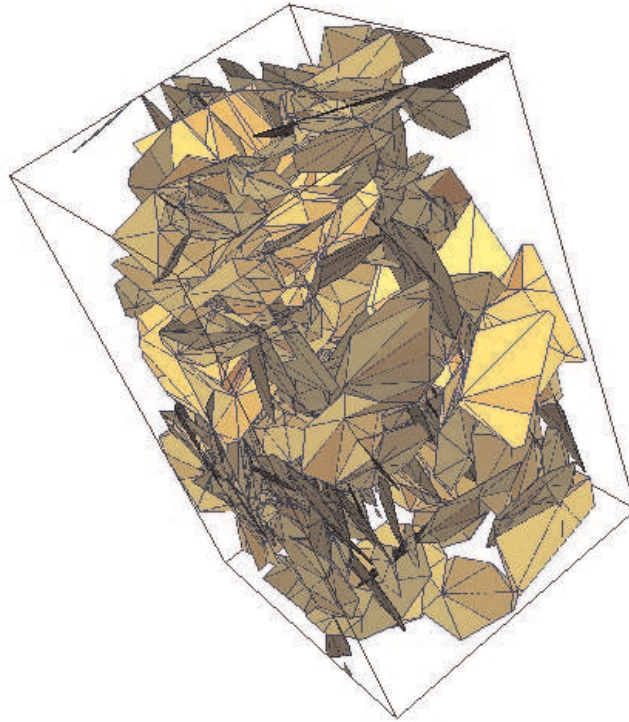


Figure 7. Triangulation of the network from Figure 3

Natural three-dimensional fractures have varying apertures. Consequently, flow is not evenly distributed within the fracture planes. So-called channels of flow occur. In order to simulate this *channeling effect*, an on-element aperture distribution function is used after the discretization. It assigns to each triangular element an aperture. Based on this aperture, the hydraulic permeability of the element is set, also taking into account the fracture wall roughness and filling. The final triangular mesh of the network from Figure 3 can be seen in Figure 7. The colours represent various values of the hydraulic permeability assigned to individual elements.

8. An example of a real problem

In this section we give an example of fracture flow around the explorational drill hole Ptp-3 in the granitoid massif of Potůčky, Western Bohemia. An almost complete set of input data for the *Fracture Net-*

Table II. Statistical characteristics of fractures with the mean orientation [0,0,1]

Depth (m)	Mean number	Std. dev. of the number	Mean of the ln of length (m)	Std. dev. of the ln of length (m)	Fish. distr. par.
0–60	64.5	13	0.3	0.5	13.7
60–120	28.5	5	0.7	0.3	13.7
120–180	27	8	0.3	0.7	13.7
180–240	36	7.5	0.5	0.2	13.7

Table III. Statistical characteristics of fractures with the mean orientation [0,1,0]

Depth (m)	Mean number	Std. dev. of the number	Mean of the ln of length (m)	Std. dev. of the ln of length (m)	Fish. distr. par.
0–60	51	8	0.1	0.4	21
60–120	27	6.5	0.5	0.6	21
120–180	76.5	22.5	0.2	0.4	21
180–240	36	10	0.7	0.2	21

work Generator was available from the results of field measurements (core-log evaluation, acoustic camera scanning, ...) given in [13]. The only missing characteristic was the distribution of fracture lengths, which has been adapted from [18]. The statistical characteristics of separate types according to their mean orientation are given in Tables II–IV. The fracture network covered a domain of 5x5x3 meters and consisted of 206 fractures, which were discretized into approx. 4000 triangular elements. The intention was to simulate fracture flow in the immediate vicinity of the borehole as precisely as possible; we also wanted to have a very small number of elements to make many tests easily possible.

8.1. PROBLEM SETTING AND BOUNDARY CONDITIONS

We have solved the problem with various boundary conditions, sources distribution, and prescribed material properties in order to check the performance of the model. We have used the *testing setting*, where the hydraulic conductivity of the elements is given in the magnitude of 1

Table IV. Statistical characteristics of fractures with the mean orientation [1,0,0]

Depth (m)	Mean number	Std. dev. of the number	Mean of the ln of length (m)	Std. dev. of the ln of length (m)	Fish. distr. par.
0–60	21	4	0.3	0.3	11.5
60–120	24	7.5	0.7	0.2	11.5
120–180	28.5	7	0.5	0.2	11.5
180–240	26.4	11.5	0.5	0.5	11.5

to 0.1 m/day and the differences between piezometric heads prescribed for the sides with Dirichlet boundary conditions are in the magnitude of the geometrical distances of these sides, and the *real setting*, where these quantities were set, respectively, to 10^{-4} – 10^{-7} m/day and 10^{-3} m.

8.2. ADJUSTMENT OF THE MESH

Obviously, one can only simulate a connected fracture system. On the other hand, the existence of fractures or sets of fractures which are not connected to the rest of the network is a natural characteristic of rock massifs, hence their existence in the generated network. As we are only interested in flow in the whole massif, exclusion of unconnected subsystems was used. The final mesh had 166 fractures and 3368 elements.

8.3. RESULTS

The results of the problems with the testing setting have the same nature as the results of the same problems with the real setting, which shows the linearity of the model. The difference between these results is proportional to the difference of the boundary conditions and permeability. This makes it possible to use the scaling of real problems.

Next, the hypothesis that the majority of flow is only conducted by a small number of fractures was confirmed. These fractures create several channels of flow in the massif, and the flux through the other fractures is negligible. The results are documented in Tables V and VI, where the distribution of the average velocity of flow over fractures, mesh elements respectively for the testing setting is shown. The average velocity of flow in the whole mesh was 0.032 m/day.

The same distribution of flow as in the whole mesh can be observed in particular fractures. In each fracture there exist one or two channels

Table V. Average velocity in fractures

Velocity [m/day]	Number of fractures
$> 10^{-1}$	13
$10^{-2} - 10^{-1}$	56
$10^{-3} - 10^{-2}$	32
$10^{-4} - 10^{-3}$	12
$< 10^{-4}$	53

Table VI. Average velocity in elements

Velocity [m/day]	Number of elements
$> 10^{-1}$	297
$10^{-2} - 10^{-1}$	1048
$10^{-3} - 10^{-2}$	794
$10^{-4} - 10^{-3}$	323
$< 10^{-4}$	906

of flow and the flux through the rest of the fracture is almost equal to zero. This situation is shown in Figure 8. Inter-element fluxes are viewed as two parallel lines and the distribution of the piezometric head is interpolated and viewed with the help of the GWS viewer system. The intersections with neighboring fractures are depicted as thick red lines. Finally, Figure 9 shows the distribution of the piezometric head in the whole simulated fracture network, for the case of the testing setting and for flow from the upper left to the lower right corner of the simulated domain.

9. Conclusions

In the present paper we have used a mixed-type finite element method to solve a locally second-order elliptic problem on a fracture network with a discontinuous permeability tensor. This ensures good accuracy of the velocity field and the fact that the mass balance is satisfied on each element. The hybrid version of the mixed finite element method of Raviart and Thomas produces symmetric and positive definite matrices. It applies directly to an arbitrary number of fractures intersecting through one edge. This is another advantage in comparison with the original mixed formulation for fracture networks, where the velocity

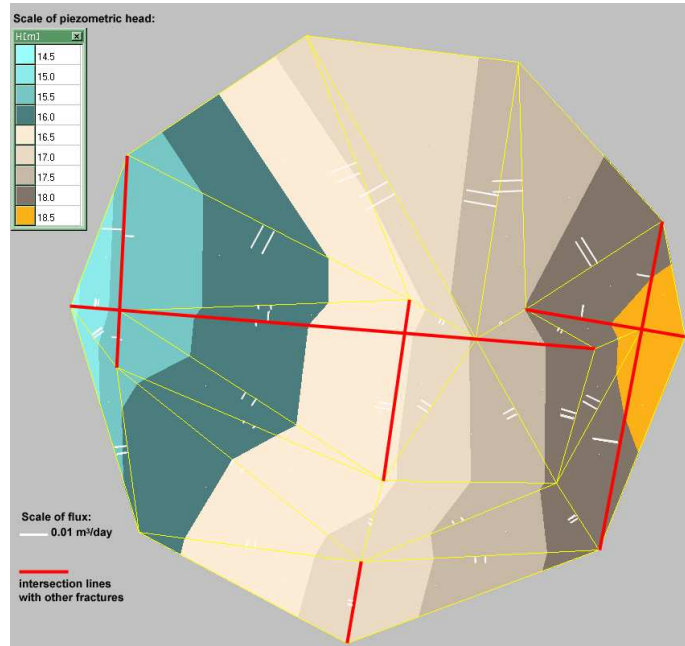


Figure 8. Flow in one fracture

basis functions for multiply shared edges are quite complicated, see [20]. The presented model problem demonstrates the validity of classical error estimates even on fracture networks.

The performed simulations of the real situation have proved good correspondence between observed phenomena and numerical approximations. The model gives an accurate velocity field within fracture planes and thus in the whole simulated network. Namely, the channeling effect was observed both in fracture planes and in the entire network. In order to obtain good-quality meshes, the use of the proposed geometrical simplifications seems essential. The three-dimensional geometrical correspondence vanishes, but the mesh is much simpler and still approximates the simulated fracture network accurately. For the mixed-hybrid finite element method, the element edges correspondence is sufficient. However, only the simulation of small domains is possible with the introduced model. To simulate large scale domains, we plan to use an equivalent porous-block approach as in [11]. In this approach one uses an equivalent porous medium model, where the permeability tensors of the elements of the partition are set up based on local stochastic discrete fracture network models.

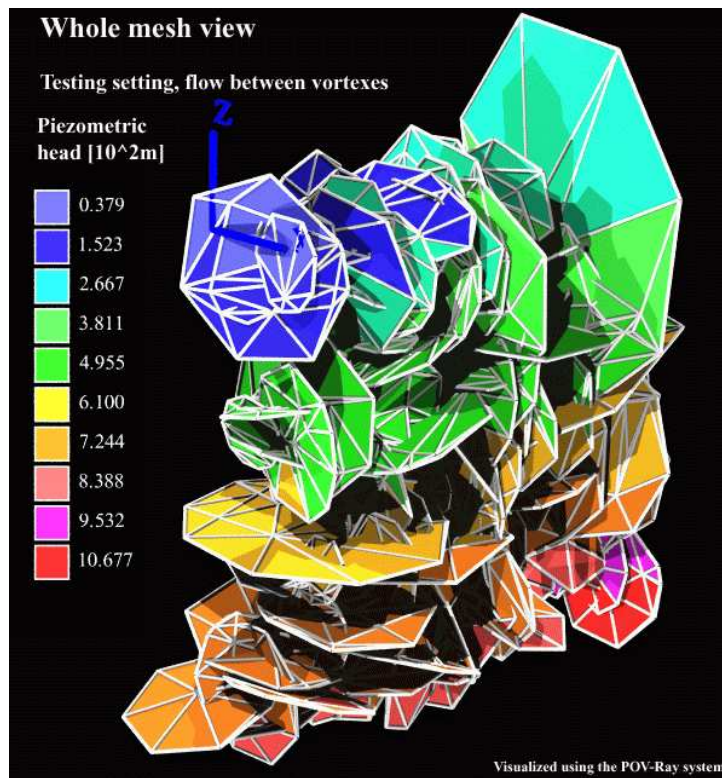


Figure 9. Distribution of the piezometric head in the fracture network

In the near future, our main interest is the simulation of contaminant transport in fracture networks. We plan to consider a nonlinear convection–reaction–diffusion equation to simulate miscible displacements.

Acknowledgements

This project was supported by the Ministry of Education of the Czech Republic, project code MSM 242200001, and by the Grant Agency of the Czech Republic under grant No. 205/00/0480. The last author was also supported by the project No. J04/98:210000010 of the Government of the Czech Republic and by the doctoral grant CTU 0212714 of the Czech Technical University in Prague. The authors would like to thank the referees for their useful suggestions.

References

1. P.M. Adler and J.-F. Thovert, *Fractures and Fracture Networks* (Kluwer Academic, Dordrecht, 1999).
2. J. Andersson and B. Dverstorp, Conditional simulations of fluid flow in three-dimensional networks of discrete fractures, *Water Resour. Res.* 23 (1987) 1876–1886.
3. P. Bastian, Z. Chen, R.E. Ewing, R. Helmig, H. Jakobs, and V. Reichenberger, Numerical simulation of multiphase flow in fractured porous media, in: *Numerical Treatment of Multiphase Flows in Porous Media*, eds. Z. Chen, R.E. Ewing, and Z.C. Shi (Springer-Verlag, Berlin, 2000) pp 50–68.
4. J. Bear, Modeling flow and contaminant transport in fractured rocks, in: *Flow and Contaminant Transport in Fractured Rock*, eds. J. Bear, C.F. Tsang, and G. de Marsily (USA: Academic Press, 1993) pp. 1–38.
5. I.I. Bogdanov, V.V. Mourzenko, J.-F. Thovert, and P.M. Adler, Effective permeability of fractured porous media in insteady state flow, *Water Resour. Res.* 39 (2003), 1023, doi:10.1029/2001WR000756.
6. F. Brezzi and M. Fortin, *Mixed and Hybrid Finite Element Methods* (Springer-Verlag, New York, 1991).
7. M.C. Cacas, E. Ledoux, G. de Marsily, B. Tillie, A. Barbreau, E. Durand, B. Feuga, and P. Peaudecerf, Modeling fracture flow with a stochastic discrete fracture network: calibration and validation 1. The flow model, *Water Resour. Res.* 26 (1990) 479–489.
8. W.S. Dershowitz and C. Fidelibus, Derivation of equivalent pipe network analogues for three-dimensional discrete fracture networks by the boundary element method, *Water Resour. Res.* 35 (1999) 2685–2691.
9. D. Elsworth, A hybrid boundary element-finite element analysis procedure for fluid flow simulation in fractured rock masses, *Int. J. Numer. Anal. Methods Geomech.* 10 (1986) 569–584.
10. N. Koudina, R. Gonzalez Garcia, J.-F. Thovert, and P.M. Adler, Permeability of three-dimensional fracture networks, *Phys. Rev. E* 57 (1998) 4466–4479.
11. P.R. La Pointe, P. Wallmann, and S. Follin, *Estimation of Effective Block Conductivities Based on Discrete Network Analyses Using Data from the Äspö Site*, Technical Report 95-15, Swedish Nuclear Fuel and Waste Management Co, Stockholm, (1995).
12. J.C.S. Long, P. Gilmour, and P.A. Witherspoon, A model for steady state flow in random three dimensional networks of disc-shaped fractures, *Water Resour. Res.* 21 (1985) 1105–1115.
13. G. Maros, K. Palotás, B. Koroknai, E. Sallay, G. Szongoth, Z. Kasza, and L. Zilahi-Sebess, *Core Log Evaluation of Borehole Ptp-3 in the Krušné hory Mts*, MS Geological Institute of Hungary, Budapest, (2001).
14. J. Maryška, M. Rozložník, and M. Tůma, Schur complement reduction in the mixed-hybrid approximation of Darcy’s law: rounding error analysis, *J. Comput. Appl. Math.* 117 (2000) 159–173.
15. J. Maryška, M. Rozložník, and M. Tůma, Schur complement systems in the mixed-hybrid finite element approximation of the potential fluid flow problem, *SIAM J. Sci. Comput.* 22 (2000) 704–723.
16. J.E. Roberts and J.-M. Thomas, Mixed and hybrid methods, in: *Handbook of Numerical Analysis, vol. 2*, eds. P.G. Ciarlet and J.L. Lions (Elsevier Science B.V., Amsterdam, 1991) pp. 523–639.

17. K.J. Slough, E.A. Sudicky, and P.A. Forsith, Numerical simulations of multi-phase flow and phase partitioning in discretely fractured geological media, *J. Contam. Hydrol.* 40 (1999) 107–136.
18. R. Stanfors, P. Olsson, and H. Stille, *Äspö HRL—Geoscientific Evaluation 1997/3*, Technical Report 97-04, Swedish Nuclear Fuel and Waste Management Co, Stockholm, (1997).
19. M. Vohralík, *Existence- and error- analysis of the mixed-hybrid model of the fracture flow*, Technical Report MATH-NM-06-2001, Dresden University of Technology, Dresden, (2001).
20. M. Vohralík, J. Maryška, and O. Severýn, Mixed-hybrid FEM on a system of polygons: application to a discrete fracture network model, to appear.
21. Z. Wanfang, H.S. Wheater, and P.M. Johnston, State of the art of modelling two-phase flow in fractured rock, *Envir. Geol.* 31 (1997) 157–166.

Address for Offprints:

Martin Vohralík
Laboratoire de Mathématiques, Bâtiment 425
Université de Paris-Sud
91405 Orsay
FRANCE
E-mail: martin.vohralik@math.u-psud.fr
Tel: +33 6 73 20 47 96
Fax: +33 1 69 15 67 18